Evaluation of Methods for Focussing Elastic Waves in Leading Edge Structures

Davide Raffaele[1,2*], Timothy Waters[1] and Emiliano Rustighi[2]

[1*]Institute of Sound and Vibration Research, University of Southampton, Southampton, SO17 1BJ, United Kingdom.
[2]Dipartimento Ingegneria Industriale, Università degli Studi di Trento, Trento, 38123, Italy.

*Corresponding author(s). E-mail(s): davide.raffaele@unitn.it;

Abstract

Wings and other aircraft lifting surfaces must remain free of ice during flight to maintain aerodynamic performance and ensure safety. Conventional de-icing approaches, such as engine bleed air, are effective but energy-intensive, motivating the exploration of alternative low-energy approaches that employ high-amplitude shock or vibration. A recently proposed method, demonstrated to delaminate an ice substitute from a beam, generates a localised shock response by focusing elastic waves in both time and space using a single actuator. However, this method requires prior knowledge of the dispersion characteristics of the waves. This study compares several wave-focusing techniques and extends their application to a semi-cylindrical structure resembling an aircraft wing leading edge. A semi-analytical finite element (SAFE) model is used to predict dispersion relations and transient responses, forming the foundation for a systematic evaluation of time-reversal and related techniques. A parametric study examines the effects of excitation bandwidth, propagation distance, and structural damping on focusing performance. Two definitions of the amplification factor are introduced, showing that dispersion compensation greatly improves the localised response. The findings not only advance low-energy de-icing strategies but also provide broader insights into wave-focusing methods applicable to dispersive media in acoustics and vibration.

Keywords: Wave focussing, Time reversal, Elastic waves, Leading edge structures, Energy amplification, Structural vibration.

1 Introduction

Aircraft icing during flight has been a concern since the very early years of aviation. The precise curvature of the wings generates a specific amount of lift, which is critical for take-off and landing performance. Any alteration in the shape of the wings or other lifting surfaces can lead to significant issues, such as increased drag and reduced lift, resulting in a loss of aerodynamic performance and controllability. Conventional ice protection systems, including pneumatic boots, electro-thermal heaters, glycol-based fluids, and bleed-air extraction, are widely used but face drawbacks in terms of weight, cost, complexity, maintenance, or power demand [1]. To address these challenges, various electromechanical de-icing systems, also known as Low-Power De-Icing (LPDI) systems, have been developed over the years to reduce the power required for ice protection during flight [1, 2]. These low-energy solutions use mechanical pulses or vibrations to break the bond between the ice accretion and the aircraft structure. The origin of LPDI systems can be traced back to 1937 when Goldschmidt [3] introduced the first Electro-Impulse De-Icing (EIDI) system. This technology employs large impulsive forces generated by electromagnetic coils on the wing's leading edge to delaminate and expel ice accretion. However, it has limitations, including electromagnetic interference, structural fatigue, and passenger discomfort due to noise [4, 5]. The Electro-Mechanical Expulsion Deicing System (EMEDS) operates on a similar principle to the EIDI and was developed by COX Inc. A short high current electrical pulse is delivered to the actuators generating opposing electro-magnetic fields that impart an impulsive repelling force that shatters and removes the ice accretion from the erosion shield [1]. Compared to traditional systems, EMEDS provides efficient ice protection at lower power levels. However, like most mechanical de-icing systems, it leaves ice residual on the surface, making it unsuitable for high-performance wings.

Recent research has focused on the use of piezoelectric actuators to remove ice accretion by inducing large vibration fields. Adachi et al. [6] were the first to propose using ultrasonic waves for ice removal. Ultrasonic de-icing concepts rely on transverse shear stresses that exceed the adhesion strength between ice the host structure. Over the years, various studies have been conducted [7–9], though findings suggest that ice delamination was sometimes primarily caused by actuator heating rather than shear stress. Subsequent research at Pennsylvania State University (PSU) concentrated on de-icing rotorcraft wings [10–13], with key limitations stemming from the insufficient force generated by piezoelectric actuators and the need to drive them at resonance, which caused heating and cracking. In his 2014 review paper [14], Palacios summarised de-icing experiments conducted at PSU, highlighting issues with actuator bonding and the fracturing of piezoelectric ceramics. He also noted the potential benefits of transient excitation over harmonic excitation.

The effectiveness of any impulsive actuator in removing ice is constrained by wave attenuation due to structural damping, wave scattering at discontinuities, and pulse dispersion during propagation. The latter is due to the dispersive nature of guided waves, characterised by the dependence of their velocity on frequency, which causes the signal to have a longer duration and lower amplitude as it travels. To mitigate the effects of wave dispersion, several signal processing techniques have been developed. Most rely on the reversibility of acoustic wave propagation, meaning the time-reversed

version of an incident pressure field naturally refocuses on its source. Time reversal, extensively applied by Fink in acoustics [15, 16], consists of a two-step process. In the forward step, a signal is launched into a medium from a source and detected along its propagation path by one or more transducers, forming a Time Reversal Mirror (TRM). In the backward step, the measured responses are time-reversed and retransmitted into the medium, compensating for wave dispersion, with the received signal closely resembling the original one.

The versatility of the time reversal technique across various fields and applications has prompted researchers to explore methods to enhance the focussing of wave energy. Deconvolution, or inverse filtering, is a method that has been used in time reversal experiments to enhance the quality of a focal signal or improve the quality of source reconstruction [17]. Anderson et al., in their experiments, demonstrated the ability of the deconvolution technique to improve both temporal and spatial focussing compared to standard time reversal [18]. However, it was found that the improved quality of the focal signal comes at the expense of reduced focal amplitude. A technique used in time reversal experiments to increase focal signal amplitude is the one-bit method, introduced by Derode et al. [19, 20]. Unlike standard time reversal, which retransmits both instantaneous phase and amplitude information, the one-bit method retransmits only the sign of the time-reversed signal. In experiments conducted in a water tank, Derode et al. achieved a 12 dB increase in the peak amplitude of the pulse using the one-bit method, while maintaining the same time compression and spatial resolution. In a recent study by Willardson et al. [21], several time reversal methods, including the aforementioned deconvolution and one-bit techniques, were compared with the objective of achieving the highest possible amplitude focus in a reverberation chamber. The study found that clipping [22], a method similar to one-bit time reversal, yielded the highest focal amplitude.

An interesting aspect of the dispersive nature of guided waves is that it can not only be compensated for but also exploited to generate a highly impulsive response at a target location [23, 24]. Waters [25] employed a simpler approach to time reversal, utilising a transient chirp excitation to focus flexural waves in a uniform beam or plate. By leveraging prior knowledge of the dispersion relation of a single wave type, a chirp waveform was analytically derived by selecting an instantaneous frequency that enables the synchronous arrival of all frequency components at an arbitrary focal point. This approach demonstrated the capability to delaminate an ice substitute from a beam; however, extension of this method to realistic wing structures requires prior knowledge of free wave propagation along the wing's leading edge, where ice typically accumulates. Moreover, the technique is difficult to extend to structures in which multiple waves can propagate.

The present work compares some wave focussing techniques available in the literature and extends their application to a semi-cylindrical structure, designed to resemble an aircraft wing slat leading edge. Furthermore, it seeks to evaluate the extent to which compensating for wave dispersion enhances the response relative to a reference excitation. Section 2 of this paper presents a semi-analytical finite element (SAFE) model of such a structure, from which the number, type and dispersion characteristics of freely propagating waves can be predicted. The source-receiver configuration used

to compute the forced response, along with the hysteretic damping model, is also presented. Section 3 introduces four different techniques for dispersion compensation. In Section 4, these techniques are applied to the SAFE model and their results are compared. Amongst them, the time reversal method is used to conduct a parametric study that investigates the effects of key parameters on wave focussing. Two distinct definitions of amplification factor are also introduced to quantify the potential amplification in shock response achieved by compensating for wave dispersion.

2 SAFE model of an aircraft wing slat leading edge structure

This section presents the SAFE model developed to predict the dispersion characteristics and forced response of the wing slat leading-edge structure considered in this study. The SAFE method is a semi-analytical numerical approach well suited for modelling elastic wave propagation in uniform, one-dimensional structures with arbitrary cross-sections. It requires discretising only the 2D cross-section using a finite-element-based procedure and applying an analytical space-harmonic solution along the propagation direction, resulting in a linear eigenvalue problem in frequency and wavenumber. The SAFE framework introduced here will be used for the wave focussing analyses presented in the following sections.

2.1 Model

In flight, wings and other aircraft lifting surfaces must be kept free from ice to maintain aerodynamic performance and controllability. With the intent of extending the deicing method presented in [25] to realistic wing structures, early activities focussed on the SAFE modelling of a Boeing 737 wing slat [26]. However, the high level of measured wave attenuation due to the presence of several internal discontinuities led to the design of a more simplistic structure that resembles its wing slat leading edge.

The new structure, hereafter referred to as wing slat leading edge, has a cross-section composed of a rectangular plate 100 by 10 mm, and a half-round plate with a diameter of 100 mm and a skin thickness of 1.2 mm. It is made of aluminium alloy ENAW-5083 and its material properties are: $\rho = 2660$ kg/m^3, $\nu = 0.33$ and $E = 70$ GPa.

In Figure 1a-1b are shown, respectively, the cross-section of the SAFE model and the finite element mesh used for the simulations. The mesh consists of 16 four-sided elements which use quadratic Lagrange shape functions, resulting in a total of 88 nodes and 264 DOFs.

The following SAFE model results have been obtained through the SAFE method implementation for free and forced wave propagation presented in [27]. This approach enables the extraction of the global mass and stiffness SAFE matrices from the finite element software COMSOL Multiphysics and the computation of free and forced responses of any arbitrary waveguide directly from the Matlab environment. This SAFE approach has been implemented for this structure and validated both numerically [27] and through an experimental method of wavenumber estimation on a laboratory structure [28]. These results are omitted from the present paper for the

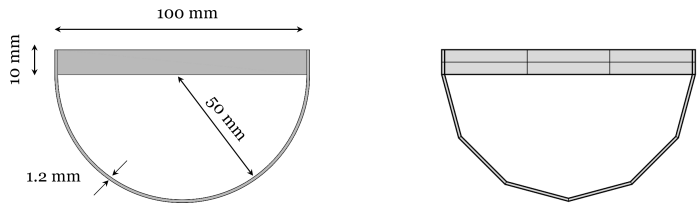

Fig. 1: SAFE model of the waveguide used to represent an aircraft wing slat leading edge: (a) cross-section, and (b) mesh.

sake of conciseness. It should be noted, however, that the proposed model can also be implemented using a standard finite element method.

2.2 Free wave propagation

Once the geometry, mesh, and frequency range are established, the SAFE method allows predicting all the possible elastic waves that may propagate in the waveguide, together with the velocities and other wave properties of interest. The eigenvalue problem yielded by the SAFE method was solved for a set of frequencies from 0 to about 16 kHz and a frequency resolution of 4 Hz.

In Figure 2 are shown the corresponding dispersion curves of the propagating waves in the form of energy velocities against frequency. No structural damping was considered in the model; therefore, all the wavenumbers are purely real above the cut-on frequencies of their respective wave modes. As one can notice, within the chosen frequency range, the SAFE model predicts the presence of four zero-order wave modes, which propagate at all frequencies, and eight higher-order wave modes of which the first four cut on at about 2, 3, 5 and 8 kHz, respectively. The zero-order wave modes consist of two bending modes, a torsional and a compressional mode.

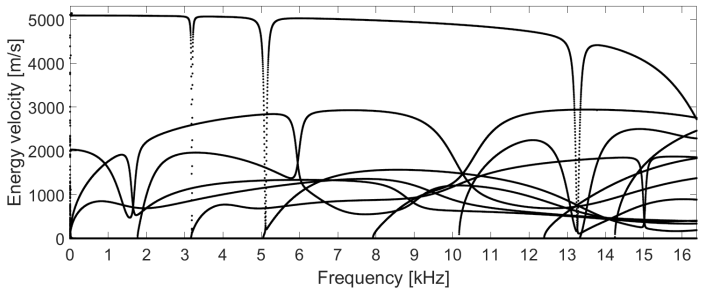

Fig. 2: Energy velocity against frequency for the propagating waves of the undamped wing slat leading edge predicted by the SAFE method.

Almost all the waves predicted by the SAFE method are dispersive. A few waves are seen to approach a velocity of about 3 and 5 km/s, which corresponds, respectively, to the speed of pressure waves and shear waves in the bulk material, while many others share a similar value of energy velocity at higher frequencies. Moreover, the obtained dispersion curves are widely characterised by the occurrence of a particular dispersion phenomenon known as *mode veering* [29, 30], which manifests when, in the proximity of some critical frequency, two branches of the dispersion curves with slopes of the same sign, instead of crossing, suddenly veer apart and swap their trajectories. For a detailed analysis of the wave mode shapes and mode veering the reader is referred to [28].

2.3 Forced wave propagation

The SAFE method can also be used to predict the forced response in the frequency domain of any node of the cross-section at any arbitrary distance from the applied loads along the direction of propagation [27].

Depicted in Figure 3 is an example of source-receiver configuration used in the following simulations. A concentrated load, p, is applied normally to the curved profile of the cross-section on point A, located at 60 degrees from the rectangular plate component. The acceleration response, a_B, is detected on point B at a distance of 2 metres from the applied load along the propagation path. It is worth noting that, in this example, points A and B correspond to the same cross-section node of the SAFE mesh. Furthermore, the choice of the excitation point is motivated by the fact that, in practical de-icing scenarios, ice debonding must occur at the wing's leading edge (i.e., the curved region), where ice tends to accumulate.

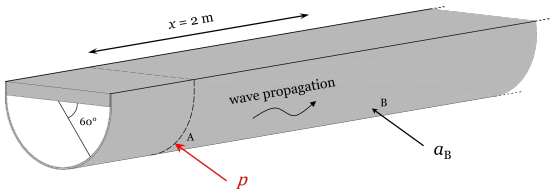

Fig. 3: Example of source-receiver configuration for the SAFE model of the wing slat leading edge. A single load is applied normally to the curved profile on point A, located at 60 degrees from the bonded rectangular plate component. Acceleration of a single node in the same circumferential position is predicted 2 metres away from the source.

2.4 Structural damping

To account for energy loss within the material, some structural damping is next introduced in the wing slat leading edge through the hysteretic model. The complex stiffness tensor is obtained by adding imaginary parts, in small percentages, to the Lamé's constants λ and μ of the material [31]. Thus, the "damped" constants for the hysteretic

model λ_D and μ_D are defined as

$$\lambda_D = \lambda\,(1 + \vartheta_\lambda j) \tag{1}$$

and

$$\mu_D = \mu\,(1 + \vartheta_\mu j)\,, \tag{2}$$

where ϑ_λ and ϑ_μ are the imaginary part added to the Lamé's constants of the undamped material.

A noteworthy point to be made is that being a frequency domain damping model, it can result in acausality for time domain simulations; however, it is likely to be insignificant for low damping values. Alternatively, acausality can be mitigated by enforcing Hermitian (conjugate) symmetry on the complex Lamé constants at positive and negative frequencies, thus ensuring real-valued, causal time-domain responses [32]. Finally, since the damping loss factor is constant at all frequencies, the response is expected to be increasingly attenuated as the frequency increases.

3 Wave focussing methods

This section introduces four wave-focusing methods reported in the literature, which are subsequently applied to the previously presented wing slat leading edge. These approaches modify the impulse response or transfer function with the objective of enhancing the focal amplitude or improving the focusing quality.

3.1 Time reversal

Time reversal (TR) has been widely used in acoustics attracting the attention of researchers in different fields of applications such as Non-Destructive Testing (NDT), medicine, communications, seismology, etc [22]. This technique is often used to generate an impulse-like focus of energy at a target position and consists of a two-step process.

In the forward step, the response to an impulse is obtained between a source and a receiver, positioned at a point A and B, respectively. In the backward step, the received signal is reversed in time and sent back through the waveguide from point B to A. The result is a time-compressed, high amplitude shock response at the initial source location A similar to the original excitation waveform.

The focal signal, $r(t)$, obtained at the initial source location A after the backward step can be expressed, in the frequency domain, as

$$R(\omega) = \Big(F(\omega)\; H(\omega)_{_{AB}}\Big)^{*}\; H(\omega)_{_{BA}} \tag{3}$$

where $F(\omega)$ is the spectrum of the initial excitation, * denotes the complex conjugate, that in the frequency domain corresponds to the time reversal operation, while $H_{_{AB}}$ and $H_{_{BA}}$ are the frequency response function (FRF) between point A and B during the forward and backward step, respectively. By using the spatial reciprocity relation

it results that $H(\omega)_{AB} = H(\omega)_{BA} = H(\omega)$, thus Equation (3) may be rewritten as

$$R(\omega) = F^*(\omega)\ |H(\omega)|^2\ . \tag{4}$$

The focal signal may be then obtained by computing its inverse Fourier transform as

$$r(t) = \mathcal{F}^{-1}\Big(F^*(\omega)\ |H(\omega)|^2\Big)\ . \tag{5}$$

Equation (5) highlights how the focal signal received at the initial source location, after the backward step, corresponds to a filtered version of the initial excitation. In particular, the time reversal process scales the spectrum of the initial excitation by the squared magnitude of the FRF while preserving its phase (with changed sign) [23].

It is worth mentioning that, another approach often used in acoustics for achieving time reversal focusing consists of using an array of transducers, called Time Reversal Mirror (TRM), placed along the wave propagation path. Each transducer detects the signal emitted from a desired source location, time-reverses it, and re-transmits it into the medium resulting in a compensation of wave dispersion with the received signal at the source location resembling the original one [15, 16]. Moreover, the reciprocal TR process (forward from A to B, then backward from A to B) offers an alternative implementation to the standard TR method (forward from A to B, then backward from B to A). In this paper, the reciprocal TR process using a single source transducer will be adopted.

3.2 Deconvolution

As previously mentioned, the time reversal technique is often used to generate an impulse-like focal signal in a two-step process. However, it cannot reconstruct exactly the initial excitation waveform and this has led researchers to explore methods to improve the quality of wave focussing.

Deconvolution, or inverse filter, is a time reversal method that provides the desired excitation signal to be used during the backward step to reproduce an approximate delta function $\delta(t)$ (limited by available bandwidth) [17, 18]. The problem of finding the required excitation, $f(t)$, necessary to approximate the focal signal, $r(t)$, to a delta function in a time reversal process may be formulated in convolution notation as

$$r(t) = f(t) \star h(t) \approx \delta(t)\ , \tag{6}$$

where $h(t)$ is the response to an impulse obtained at the receiver location in the forward step.

Deconvolution equates to inverse filter by transforming to the frequency domain, therefore Equation (6) becomes

$$R(\omega) = F(\omega)\ H(\omega) \approx 1\ , \tag{7}$$

where $H(\omega)$ corresponds to the FRF between the source and receiver location. It follows that the required excitation to use in the backward step of the time reversal

process corresponds to the frequency domain inverse of the FRF obtained in the forward step

$$F(\omega) = \frac{1}{H(\omega)} = \frac{H^*(\omega)}{|H(\omega)|^2} \ , \tag{8}$$

where $*$ denotes the complex conjugate operation.

Equation (8) provides an analytical expression for $F(\omega)$, but it may not be practical for experimental use in cases of limited bandwidth, significant background noise, or if $H(\omega)$ is close to zero at any frequency [18]. To avoid this, a constant is usually added to the denominator; thus Equation (8) is replaced by

$$F(\omega) = \frac{H^*(\omega)}{|H(\omega)|^2 + \gamma \ \mathrm{mean}\Big(|H(\omega)|^2\Big)} \ , \tag{9}$$

where γ is an arbitrary non-dimensional constant (sometimes referred to as water level [33]) chosen to reduce the effect of noise introduced through the deconvolution method. The required excitation $f(t)$ is then obtained by transforming back to the time domain.

It is worth pointing out that the enhanced quality of the focal signal comes at the expense of lower focal amplitude. In fact, whereas the time reversal method sends back a complex conjugate (or time reversal) of the forward information, the deconvolution method sends back a frequency domain inverse of the forward information. Moreover, the above derivation suggests that, by prior knowledge of the FRF between the source and receiver positions, the excitation signal necessary to recreate an approximate delta function, $\delta(t)$, at a target position can be directly computed. The procedure will then consist of just the backward step of the time reversal process. Finally, in a recent work, Anderson et al. [18] have provided an expression for deriving the necessary input signal capable of reconstructing an arbitrary source function.

3.3 One-bit time reversal

The one-bit method introduced by Derode et al. [19, 20] is a technique used in time-reversal experiments to increase the amplitude of the focal signal.

Differently from the standard time reversal procedure, where both the phase and amplitude information are retransmitted, in the one-bit method, only the sign of the time-reversed signal is sent back. The one-bit processed signal is obtained from an impulse response normalised to unit amplitude; a value between 0 and 1 is chosen as a threshold, and everything between the positive and negative threshold values is set to 0 for noise rejection. The one-bit processed signal only contains values of ± 1 and 0; however, since the phase information is preserved, the focusing is still achievable.

3.4 Clipping

Clipping, a variant of the one-bit method, was introduced by Heaton et al. [22] as an alternative signal processing method for TR.

The normalised impulse response is first intentionally clipped by applying a multiplication factor, C. Then, a threshold value of 1 is set, and every TR signal information

above the positive threshold or below the negative threshold value is set equal to 1 and -1, respectively. Differently from the one-bit method, the information that lies between the positive and negative threshold values remains unchanged.

4 Numerical results

In the following, the above wave focussing methods are applied to the SAFE model of the wing slat leading edge introduced in Section 2 using the same source-receiver configuration shown in Figure 3 with a 0.1% structural damping and a frequency bandwidth of 16 kHz. For each technique, a rectangular pulse of 0.1 ms duration is used to excite the structure, while the focal point is arbitrarily chosen at a distance of 2 metres from the source.

The time reversal method has been implemented following the reciprocal approach (forward from location A to location B and then backward from A to B) with a single source. In the forward step, the spectrum of the rectangular pulse is multiplied by the transfer accelerance FRF predicted at the chosen focal point and, by transforming back to the time domain, its response signal is obtained. Figure 4a shows the time-reversed response signal, normalised to unit peak amplitude, used as input in the backward step, while Figure 4b shows the corresponding response signal predicted at the focal point. As one can notice, due to the dispersion compensation, the response signal obtained in the backward step, Figure 4b, manifests itself as much more impulsive than the corresponding excitation waveform shown in Figure 4a.

In the deconvolution method the desired excitation waveform to be used in the backward step has been obtained by multiplying the spectrum of the rectangular pulse by the inverse of the accelerance FRF predicted at the target position and then transforming back to the time domain. For illustration purposes, a 500 Hz high-pass filter has also been applied to the desired excitation waveform. The obtained signal, Figure 4c, is then sent through the waveguide and seen progressively recombining towards the rectangular pulse as it propagates from the source. Figure 4d shows the response signal predicted at the chosen focal point. As one can notice, the rectangular pulse is not fully reconstructed at the target position; however, it can be proved that by focussing all the frequency components, i.e. with no filter applied, the exact original signal can be obtained.

Figure 4e shows the one-bit processed signal obtained from the time-reversed response signal shown in Figure 4a by using a threshold value of 0.02, while Figure 4f shows its shock response predicted at the target position.

The clipping method has been implemented by applying a multiplication factor C=50 to the time-reversed response signal shown in Figure 4a. The computed clipped signal, Figure 4g, is then sent in the backward step of the standard time reversal method obtaining, at the target position, the shock response shown in Figure 4h.

By comparing the wave focussing results shown in Figure 4, it emerges that the one-bit and the clipping TR methods are the ones capable of producing a higher focal amplitude reaching, respectively, an acceleration peak value of 8553 m/s^2 and 9164 m/s^2, much higher than the standard TR method with its 2970 m/s^2. As expected, the deconvolution TR method with its 18 m/s^2 produces the lowest response peak.

Overlaid in Figure 5a are the positive acceleration response peaks, as a function of distance from the source, obtained through the standard, one-bit, and clipping TR methods. Figure 5b shows instead the corresponding ones obtained through the deconvolution TR method to prove the achieved wave focussing notwithstanding the low focal amplitude. As one can notice, for each curve the waves are successfully focused at the chosen target position of 2 metres from the source where the maximum acceleration peaks occur. A high peak value is also observed at the source position, resulting from constructive interference of highly attenuated nearfield waves.

By looking at the focal point, the one-bit method provides an acceleration peak amplitude of about three times higher than the standard TR technique. Such amplification can be explained by comparing Figure 4a and Figure 4e. In fact, while preserving the corresponding phase information contained in the "unprocessed" impulse response, the 1-bit signal waveform has a much higher signal power that is delivered into the waveguide. In this example, the clipping TR method yields the highest response peak. This is partly due to the application of the multiplication factor and the fact that the information between the threshold values is not zeroed out, as in the one-bit processed signal. As a result, more energy is transferred into the structure.

Finally, Figure 6 shows the focal signals obtained in Figure 4 in the proximity of the focal time after being normalised to unit peak amplitude. They have been plotted against the original source function to compare accurately their temporal compression. Amongst them, the deconvolution TR focal signal overlays the rectangular pulse, exhibiting the highest temporal compression. This demonstrates how the enhanced focal quality obtained by the deconvolution TR method comes at the expense of lower focal amplitude. To overcome this limitation and thus achieve high focal amplitude without renouncing to the focal quality, the literature provides examples where one-bit or clipping TR methods are applied to the deconvolution TR signal [21, 22].

However, it is important to emphasise that this section provides only an overview of some TR methods available in the literature, rather than a comprehensive comparison. A more in-depth analysis of the impact of threshold value, multiplication factor, and other parameters on focal amplitude would be required, but this lies beyond the scope of this paper.

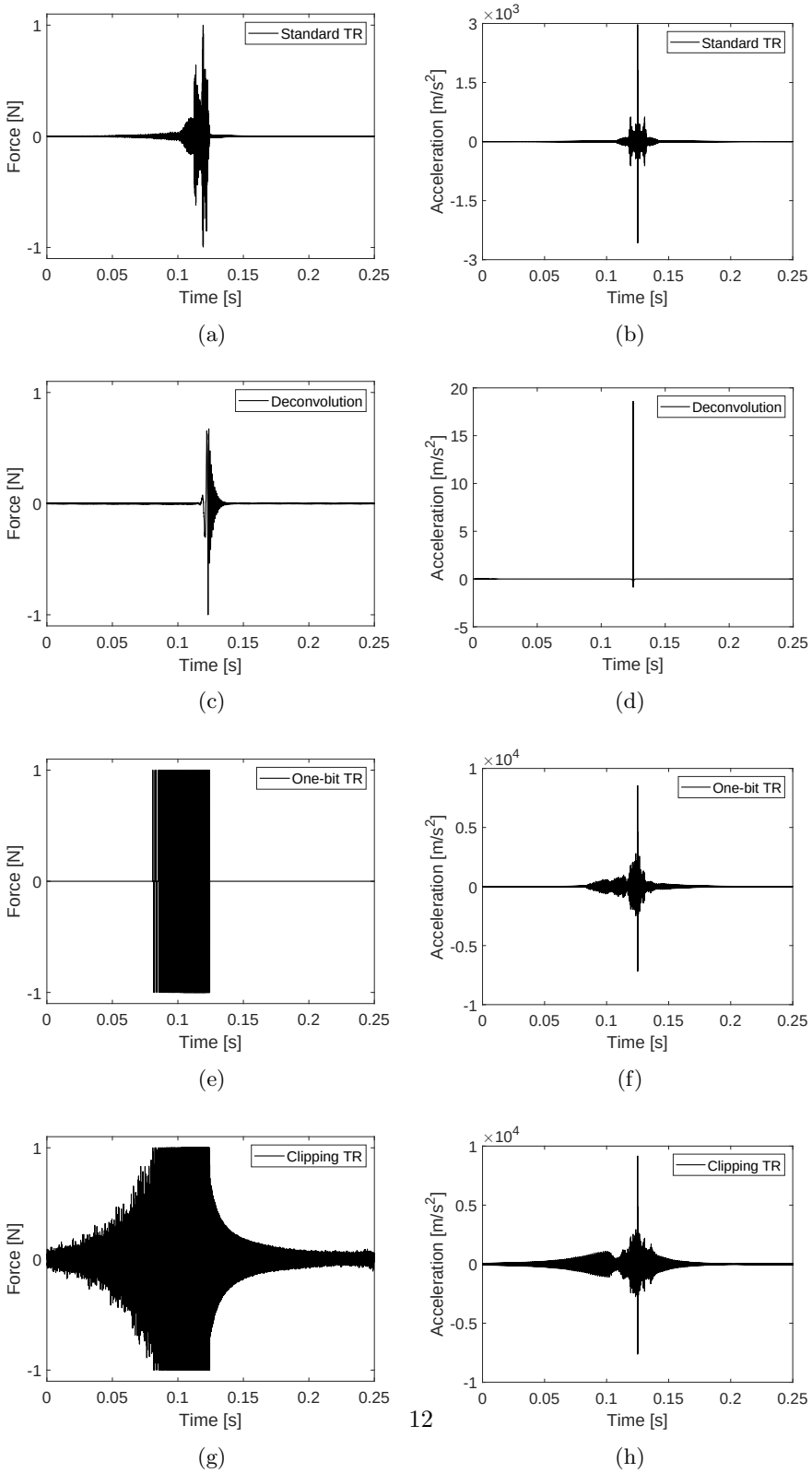

Fig. 4: Back propagation step of the TR methods herein presented for the wing slat leading edge with 16 kHz excitation bandwidth, 0.1% of structural damping, and focal point at 2 metres from the source. (a) Standard TR response signal due to a rectangular pulse of 0.1 ms duration, and (b) TR focal signal; (c) deconvolution TR signal, and (d) deconvolution TR focal signal; (e) one-bit TR signal, and (f) one-bit TR focal signal; (g) clipping TR signal, and (h) clipping TR focal signal.

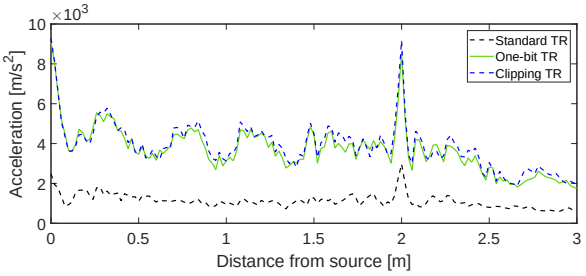

(a)

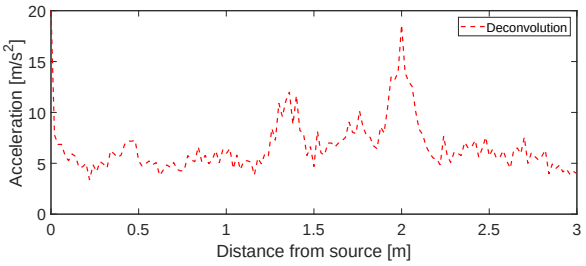

(b)

Fig. 5: Positive acceleration response peaks as a function of distance from the source of (a) the standard, one-bit, clipping, and (b) the deconvolution TR method for the wing slat leading edge with 16 kHz excitation bandwidth, 0.1% of structural damping, and focal point at 2 metres from the source.

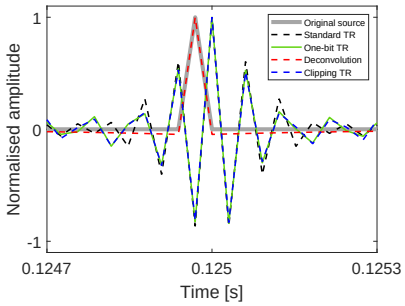

Fig. 6: Focal signals resulting from the TR methods shown in Figure 4, normalised to unit amplitude and compared with the original source function (grey solid line). The Deconvolution focal signal (dashed red line) matches the original source, illustrating the higher focal quality achieved. However, this improvement comes at the cost of the significantly lower focal amplitude shown in Figure 5b.

5 Performance of wave focussing methods

In the previous sections, some wave focussing methods from the literature have been presented and their results compared. This section, instead, aims to evaluate the extent to which compensating for wave dispersion enhances the response, relative to a reference excitation.

In particular, to account for the limitation presented by electrodynamic shakers and piezoelectric actuators when employed at high amplitudes, a comparison of the response in terms of power and peak amplitude is presented. In fact, during ultrasonic de-icing experiments piezoelectric actuators are often driven to their tensile fracture limit, causing the crack and fracture of the piezoelectric material [13].

Electrodynamic shakers, instead, when employed at higher frequencies, consume a significant electrical power that is converted to heat, which may finally result in overstressing of the armature structure and melting of the coil [34].

In the following, as an example, the performance of the standard time reversal focussing will be thus evaluated through an amplification factor in terms of power and peak amplitude obtained by comparing the time reversal response at the focal point to a harmonic and near-tonal response used as a reference.

5.1 Peak amplitude comparison

In the following, by using the standard time reversal results presented in Section 4, the performance of wave focussing is evaluated in terms of peak amplitude through comparison with a harmonic response.

Consider the accelerance FRF of Figure 7 predicted at the focal point, which in this example is at 2 metres from the source. The frequency that provides the largest response is used as a benchmark and henceforth referred to as benchmark frequency, $\mathrm{f}_{\mathrm{bench}}$.

By plotting the FRF value corresponding to such a frequency, as a function of distance from the source, the green curve shown in Figure 8 is obtained. The observed oscillations are the results of the interference of several waves with different wavenumbers excited at the benchmark frequency. Such a curve represents accelerations per unit force and, at the focal point of 2 metres, it corresponds to the largest steady-state response that one can get if the structure is excited time-harmonically at the benchmark frequency.

It is compared to the peak responses obtained by focussing energy over all frequencies through the standard TR technique. Therefore, in terms of peak amplitude, the performance of wave focussing can be assessed by the amplification factor, AF_{peak}, obtained by the ratio of the two curves at the focal point.

5.2 Power comparison

In the following, using the same standard time reversal results presented in Section 4, the performance of wave focussing is evaluated as a function of signal power. It is worth highlighting that it does not guarantee the same mechanical power, which also depends on the mechanical impedance of the structure.

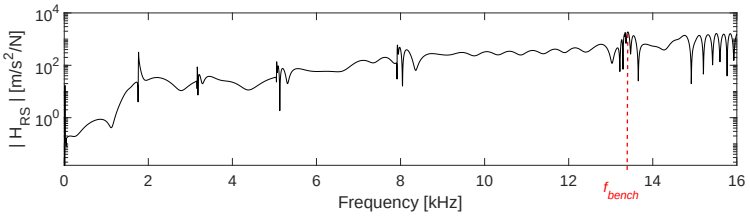

Fig. 7: Transfer accelerance FRF for the SAFE model of the wing slat leading edge with 16 kHz excitation bandwidth, 0.1% of structural damping, and focal point at 2 metres from the source. The benchmark frequency, f_{bench}, is the frequency which provides the largest response.

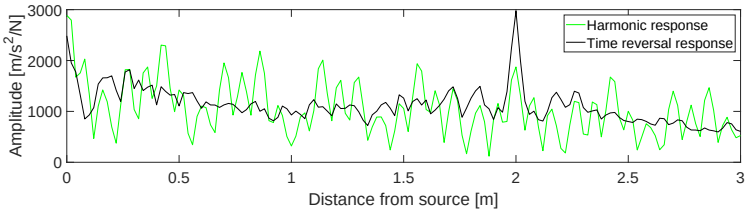

Fig. 8: Performance of wave focussing, in terms of peak amplitude, for the SAFE model of the wing slat leading edge with 16 kHz excitation bandwidth, 0.1% of structural damping, and focal point at 2 metres from the source. The harmonic response (in green), which is used as a benchmark, is obtained by plotting the FRF value corresponding to the benchmark frequency as a function of distance from the source. The amplification factor, AF_{peak}, is thus defined as the ratio of the time reversal response (in black) to the harmonic response at the focal point.

Based on the standard time reversal excitation waveform of Figure 4a, a Gaussian-windowed tone burst of comparable duration and modulated with a centre frequency corresponding to f_{bench} is computed through the Matlab "Gauspuls" function and used as a reference. The tone burst duration is determined by maximising correlation with the standard time reversal waveform. Finally, the tone burst has been scaled conveniently to have the same signal power as the time reversal excitation and used to excite the waveguide. For illustration purposes, an example of the two excitation waveforms are overlaid in Figure 9.

In Figure 10 the acceleration response peaks, as a function of distance from the source, obtained by exciting the waveguide with the tone burst are overlaid with the ones obtained through the standard time reversal technique shown in Figure 5a. Both curves have been normalised by the root-mean-square value of their excitation waveform to obtain accelerations per unit power.

At the focal point of 2 metres, the response obtained through the tone burst excitation represents the largest response that one can get by concentrating energy over a finite bandwidth centred on the benchmark frequency. This is compared to the

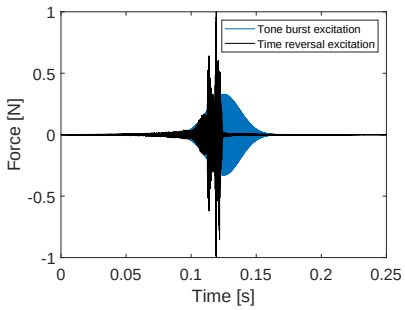

Fig. 9: Time reversal excitation waveform versus tone-burst excitation used as a reference to evaluate the performance of wave focussing. The two excitations have same power and comparable duration.

response obtained by focussing energy over all frequencies through the time reversal technique.

Thus, in terms of power, the performance of wave focussing can be evaluated by the amplification factor, AF_{power}, obtained by the ratio of the two curves at the focal point. By looking at Figure 10 and Figure 8 one can notice that the tone burst

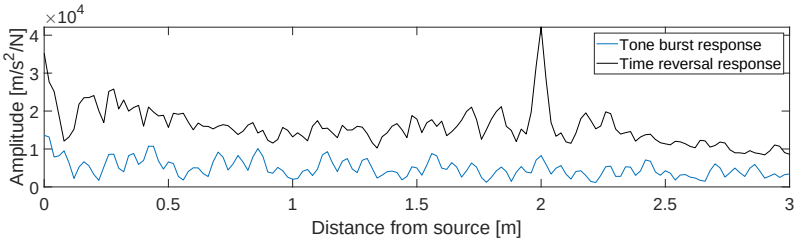

Fig. 10: Performance of wave focussing, in terms of power, for the SAFE model of the wing slat leading edge with 16 kHz excitation bandwidth, 0.1% of structural damping, and focal point at 2 metres from the source. The amplification factor, AF_{power}, is defined as the ratio of the time reversal response to the tone-burst response at the focal point.

response is much lower than that due to the harmonic excitation. An explanation can be given by the fact that not all the energy of the tone burst excitation is input at the benchmark frequency, but it is spread over a finite bandwidth.

6 Parametric study for wave focussing

Along with the direction of excitation, the frequency bandwidth, structural damping, and focal distance represent key parameters for the wave focussing. Therefore, this section aims to present a study on the effects of these parameters. The values that will be used are listed below:

- Frequency range of excitation: 8 kHz, 16 kHz and 32 kHz.
- Structural damping: 0.1% and 1%.
- Distance of focussing: 2m, 4m and 8m.

Amongst the time reversal methods herein presented, with the only intent of showing the effect of the aforementioned parameters, for brevity, only the results obtained for the standard time reversal method are presented.

It is worth highlighting that all the following simulations are obtained by using the same source-receiver configuration depicted in Figure 3 and, for brevity, only the performance in terms of peak amplitude is shown. A summary of the conducted parametric study can be found at the end of this section, where, for each simulation, the benchmark frequency and both amplification factors are reported.

6.1 Variation of excitation bandwidth

In the following, to present the effect of the excitation bandwidth, a focal distance of 2 metres from the source and a 0.1% of structural damping are fixed. Figure 11 shows the results obtained by varying the excitation bandwidth from 8 kHz to 32 kHz.

From Figure 11a it emerges that when the waveguide is excited up to 8 kHz, an amplification factor AF_{peak} of 0.7 is obtained. At the focal distance of 2 metres, the results indicate that by exciting the waveguide time-harmonically at the benchmark frequency, a higher acceleration is obtained than by focussing energy over all frequencies. A reason could be found in the destructive interference of the wave components within this frequency range.

As shown in Figure 11b - 11c, when the bandwidth is increased to 16 kHz and 32 kHz, the amplification factor rises respectively to 1.6 and 2.4. From the results it emerges that the amplification factor increases as the excitation bandwidth is increased.

An explanation can be given by looking at the transfer accelerance FRF shown in Figure 12 predicted at the focal distance of 2 metres and for a bandwidth of 32 kHz. It is evident that by focussing energy up to 8 kHz, only a few frequency components contribute to the response. Conversely, the transfer FRF shows a relatively flat response at higher frequencies, indicating that more frequency components contribute to wave focussing if the excitation bandwidth is increased.

6.2 Variation of focal distance

In the following, the effect of the focal distance on wave focussing is investigated by using an excitation bandwidth of 32 kHz and a 0.1% of structural damping. In Figure 13a,b,c are presented, respectively, the amplification factor AF_{peak} at the focal distance of 2, 4 and 8 metres from the source. The results show that the amplification factor increases as the distance of focussing is increased. At 2 metres from the source, an amplification factor of 2.4 is achieved, reaching a value of about 3 and 5 when the focal distance is increased respectively to 4 and 8 metres. The improvement occurs because an increase in focal distance results in a longer time delay between the slowest and fastest frequency components. This extends the excitation waveform's duration, introducing more energy into the system.

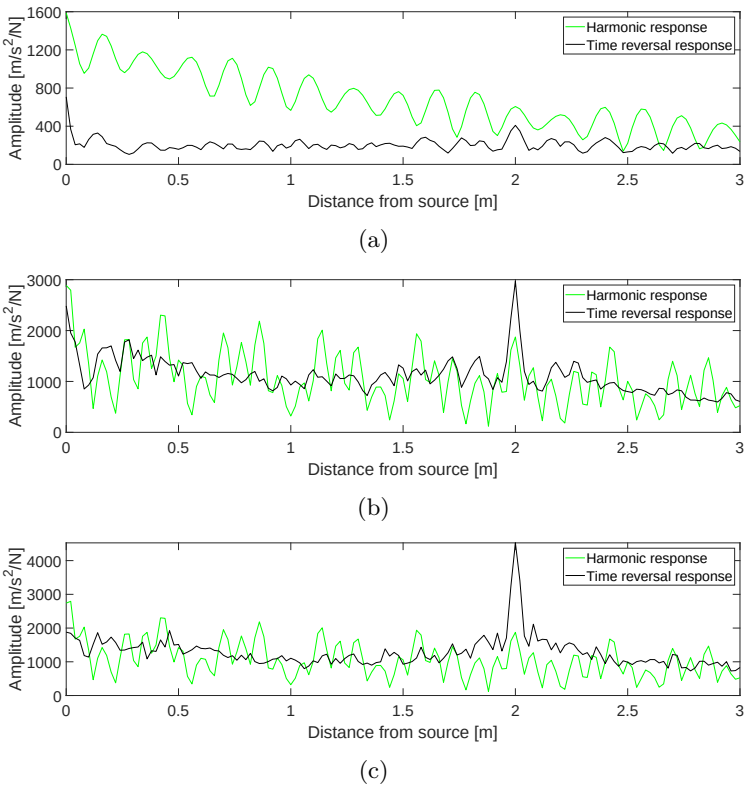

Fig. 11: Effect of excitation bandwidth on the standard TR technique: acceleration responses per unit force, as a function of distance from the source, for the SAFE model of the wing slat leading edge with 0.1% of structural damping and focal point at 2 metres. (a) 8 kHz bandwidth (AF_{peak}=0.7); (b) 16 kHz bandwidth (AF_{peak}=1.6); and (c) 32 kHz bandwidth (AF_{peak}=2.4).

Finally, it is worth noting that the presence of structural damping increasingly attenuates the response as the distance increases. The next section will examine this aspect further.

6.3 Effect of structural damping

In this example, to investigate the effect of structural damping on wave focussing, a frequency bandwidth of 16 kHz and a focal distance of 4 metres is fixed.

Figure 14 shows the variation of the amplification factor as the level of damping is increased. From the results, it is apparent that, for the same focal distance and frequency bandwidth, the amplification factor, AF_{peak}, decreases from 2.8 to 1.8 as the structural damping increases from 0.1% to 1%. As expected, attenuation is responsible for reducing amplification significantly, particularly at higher distances.

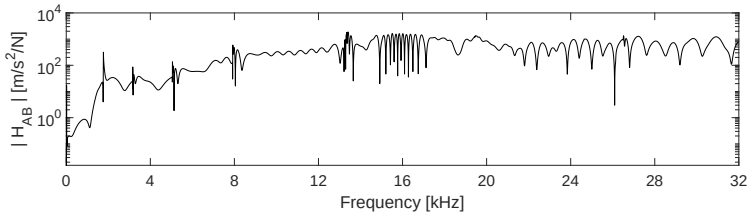

Fig. 12: Transfer FRF for the wing slat leading edge with 0.1% of structural damping, focal point at 2 metres from the source, and 32 kHz excitation bandwidth. The relatively flat response at higher frequencies indicates the benefit that can be attained by increasing the excitation bandwidth.

6.4 Summary of the parametric study

In this section, an overview of the effects of the excitation bandwidth, focal distance, and structural damping on time reversal focussing has been presented. In particular, three frequency bandwidths (approximately 8, 16, and 32 kHz), three different focal distances (2, 4, and 8 metres), and two levels of structural damping (0.1% and 1%) have been considered. All the simulations were conducted by using the same source-receiver configuration depicted in Figure 3. Table 1 summarises the obtained results indicating, for each simulation, the corresponding amplification factors and benchmark frequency.

Frequency range [Hz]	Structural damping	Focal distance [m]	AF		Benchmark frequency [Hz]
			Peak	Power	
8192	0.1%	2	0.7	0.007	7926
		4	1.0	0.01	8042
		8	0.9	0.01	8092
	1%	2	0.9	2.4	8156
		4	1.1	3.9	7350
		8	1.2	5.9	6316
16384	0.1%	2	1.6	5.1	13408
		4	2.8	8.5	13408
		8	2.9	8.8	13964
	1%	2	1.5	4.9	13428
		4	1.8	6.0	13016
		8	1.6	7.9	8744
32768	0.1%	2	2.4	9.1	13408
		4	2.9	14.0	13408
		8	4.7	15.6	13960
	1%	2	1.9	6.5	13424
		4	2.2	4.6	13016
		8	1.3	8.0	8744

Table 1: Parametric study on wave focussing obtained via the standard TR technique for the SAFE model of the wing slat leading edge.

At first sight, one can notice that both amplification factors follow a similar trend. The main difference is that the amplification factor in terms of power, AF_{power}, presents higher values than the corresponding one in terms of peak amplitude, AF_{peak}, manifesting a much lower benchmark response than the harmonic one. A reason could

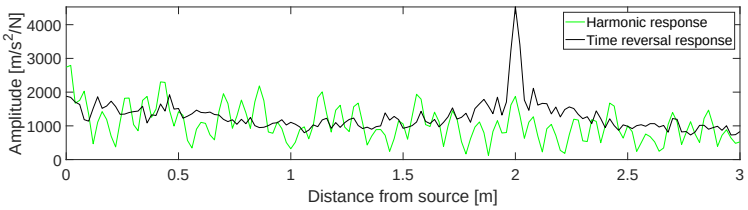

(a)

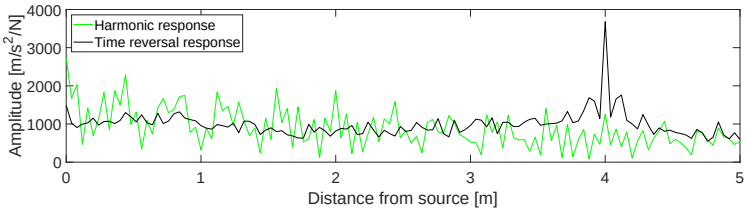

(b)

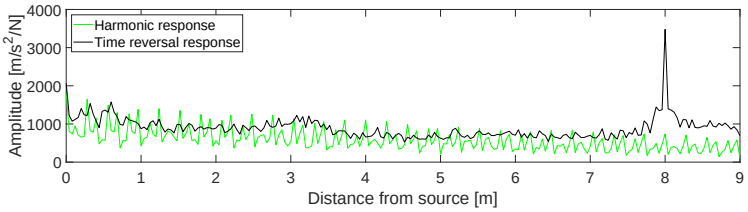

(c)

Fig. 13: Effect of focal distance on the standard TR technique: acceleration responses per unit force, as a function of distance from the source, for the SAFE model of the wing slat leading edge with 32 kHz excitation bandwidth and 0.1% of structural damping. (a) focal point at 2 metres (AF_{peak}=2.4); (b) focal point at 4 metres (AF_{peak}=2.9); and (c) focal point at 8 metres (AF_{peak}=4.7).

be that not all the energy of the Gaussian pulse is focused on the benchmark frequency, but it is spread over a finite bandwidth. Values of amplification factors less than one suggest that within the corresponding frequency range only a few frequency components contribute to the response.

By referring to the amplification factor in terms of peak response it emerged that, for the same distance and level of damping, the amplification factor increases as the excitation bandwidth is increased. An explanation was found in the relatively flat response of the FRF at higher frequencies, which indicates that more frequency components contribute non-negligible to the response. Moreover, for the same excitation bandwidth and structural damping, as the focal distance is increased an increase in the peak response was found. As shown in Figure 13, for a 0.1% of structural damping and an excitation bandwidth of 32 kHz, the amplification factor AF_{peak} varies from a value of 2.4 at a distance of 2 metres to a value of 2.9 and 4.7 respectively at 4 and 8 metres. A similar trend is observed as the structural damping is increased.

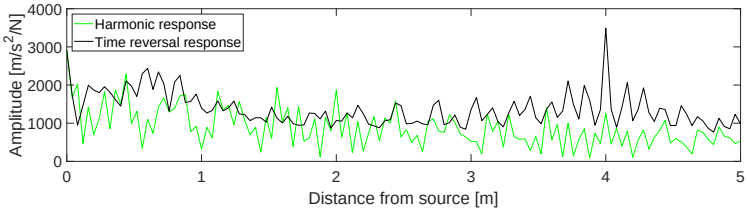

(a)

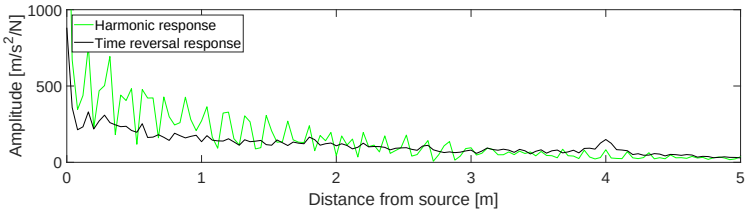

(b)

Fig. 14: Effect of structural damping on the standard TR technique: acceleration responses per unit force, as a function of distance from the source, for the wing slat leading edge with 16 kHz excitation bandwidth and focal distance at 4 metres from the source. (a) 0.1% of structural damping (AF_{peak}=2.8); and (b) 1% of structural damping (AF_{peak}=1.8).

However, once the focal distance exceeds 4 metres, a reduction in the amplification factor is observed. For example, by maintaining the bandwidth of 32 kHz and increasing the structural damping to 1%, the amplification factor AF_{peak} is seen to increase from 1.9 to 2.2 and then decrease to a value of 1.3 at the focal distance of 8 metres. As expected, attenuation is responsible for reducing the amplification, particularly at higher distances and damping levels.

The identified trends, namely the increase of amplification with excitation bandwidth and focal distance, and its reduction with damping, are consistent with fundamental dispersion compensation principles and are thus expected in other waveguides. However, the quantitative amplification values depend on the modal density and attenuation of the specific geometry. Consequently, these findings should be regarded as general expectations that require experimental validation on other structural configurations, such as composite shells or full-scale leading-edge assemblies.

7 Conclusions

This work investigated the applicability of some wave focussing techniques available in the literature (i.e. standard, deconvolution, one-bit, and clipping time reversal) to a semi-cylindrical structure representative of an aircraft wing slat leading edge for potential de-icing applications. A SAFE model of this structure was developed to predict the dispersion characteristics and the transient response at arbitrary distances

from the applied load along the wave propagation direction. Structural damping was also introduced using a hysteretic model.

From the results obtained, the deconvolution TR method showed its ability to reconstruct the original excitation waveform and focus the waves precisely at the target position. However, as expected, the enhanced quality of the focal signal came at the cost of reduced focal amplitude. Conversely, the standard, one-bit, and clipping TR methods demonstrated their ability to generate a much stronger shock response near the target location, with the clipping approach achieving a response peak at the focal point about three times higher than that of the standard TR method.

The SAFE model was then used to conduct a parametric study on the standard TR method to examine the effects of excitation bandwidth, propagation distance, and structural damping on wave focussing. To evaluate the extent to which compensating for wave dispersion enhances the response compared to a reference excitation, amplification factors in terms of input signal power and peak amplitude were defined. The results revealed that, although different in values, both amplification factors exhibited a similar trend. In particular, it was observed that, for the same focal distance and damping level, the amplification factor associated to peak amplitude increased as the excitation bandwidth was increased. The reason was found in the relatively flat response of the transfer FRF at higher frequencies, indicating that, when a broader bandwidth is excited, more frequency components significantly contribute to the response. Moreover, for the same excitation bandwidth and structural damping, an increase in the peak response was observed up to the focal distances considered. However, as expected, at greater focal distances and levels of damping, attenuation is responsible for reducing the amplification.

The observed dependence of amplification on excitation bandwidth, focal distance, and damping is consistent with the behaviour of dispersive waveguides, arising from dispersion compensation mechanisms, and is therefore applicable to other structures exhibiting similar modal characteristics. Future studies should explore its effectiveness in more complex configurations, including aircraft wings and composite materials, where attenuation may be more pronounced. The quantitative amplification factors and benchmark frequencies obtained in this study (e.g., $AF_{peak} = 4.7$ at 32 kHz over an 8 m focal distance) are specific to the semi-cylindrical aluminium structure, reflecting its geometry and material properties; these values should therefore be considered demonstrative rather than universal.

Beyond their relevance for de-icing, these findings advance fundamental understanding of wave focussing in dispersive media and highlight dispersion compensation as an effective strategy for energy localisation. Future work will involve coupling an electromechanical actuator model to the SAFE model, incorporating ice accretion to enable the prediction of interfacial stresses between the host structure and the ice, and exploring the use of multiple excitation inputs to preferentially excite selected propagation modes.

Declarations

Acknowledgements. The authors are grateful to Ultra Electronics for their financial support and acknowledge the use of the IRIDIS High Performance Computing Facility, and associated support services at the University of Southampton, in the completion of this work.

Conflict of interest. The authors declare that they have no conflict of interest.

Author Contribution. Davide Raffaele: conceptualization, methodology, software, validation, formal analysis, investigation, resources, writing – original draft, writing – review & editing, visualization. Timothy Waters: conceptualization, methodology, validation, formal analysis, investigation, resources, writing – review & editing, supervision, project administration, funding acquisition. Emiliano Rustighi: conceptualization, methodology, software, validation, investigation, resources, writing – review & editing, supervision, project administration.

References

[1] Goraj, Z.: An Overview of the De-Icing and Anti-icing Technologies with Prospects for the Future. In: 24th International Congress of the Aeronautical Sciences, vol. 29, p. 11 (2004)

[2] Krammer, P., Scholz, D.: Estimation of Electrical Power Required for Deicing Systems. Technical report, Hamburg University of Applied Sciences (2009)

[3] Goldschmidt, R.: Improvements in and Relating to De-icing Equipment, for Example for Aircraft. GB505433A, 1937

[4] Zumwalt, G.: Icing tunnel tests of Electro-Impulse De-Icing of an engine inlet and high-speed wings. In: 23rd Aerospace Sciences Meeting. AIAA, Reno, NV, U.S.A. (1985)

[5] Labeas, G.N., Diamantakos, I.D., Sunaric, M.M.: Simulation of the Electroimpulse De-Icing Process of Aircraft Wings. Journal of Aircraft **43**(6), 1876–1885 (2006)

[6] Adachi, K., Saiki, K., Sato, H.: Suppression of frosting on a metal surface using ultrasonic vibrations. In: 1998 IEEE Ultrasonics Symposium. Proceedings, vol. 1, pp. 759–762. IEEE, Sendai, Japan (1998). https://doi.org/10.1109/ULTSYM.1998.762258 . http://ieeexplore.ieee.org/document/762258/

[7] Ramanathan, S., Varadan, V.V., Varadan, V.K.: Deicing of helicopter blades using piezoelectric actuators. In: SPIE's 7th Annual International Symposium on Smart Structures And Materials, Newport Beach, CA, pp. 281–292 (2000). https://doi.org/10.1117/12.388906 . http://proceedings.spiedigitallibrary.org/proceeding.aspx?articleid=925064 Accessed 2021-05-08

[8] Venna, S.V., Lin, Y.-J.: Mechatronic Development of Self-Actuating In-Flight Deicing Structures. IEEE/ASME Transactions on Mechatronics **11**(5), 585–592 (2006) https://doi.org/10.1109/TMECH.2006.882990 . Accessed 2021-05-08

[9] Venna, S.V., Lin, Y.-J., Botura, G.: Piezoelectric Transducer Actuated Leading Edge De-Icing with Simultaneous Shear and Impulse Forces. Journal of Aircraft **44**(2), 509–515 (2007) https://doi.org/10.2514/1.23996 . Accessed 2021-05-08

[10] Palacios, J.L.: Design, fabrication, and testing of an ultrasonic de-icing system for helicopter rotor blades. PhD thesis (2008). http://adsabs.harvard.edu/abs/2008PhDT.....96P Accessed 2021-05-08

[11] Palacios, J., Smith, E., Rose, J.: Investigation of an Ultrasonic Ice Protection System for Helicopter Rotor Blades. Annual Forum Proceedings - AHS International **1** (2008)

[12] Zhu, Y., Palacios, J.L., Rose, J.L., Smith, E.C.: De-icing of multi-layer composite plates using ultrasonic guided waves. In: 49th AIAA Structures, Structural Dynamics, and Materials Conference, USA (2008). https://doi.org/10.2514/6.2008-1862 . https://pennstate.pure.elsevier.com/en/publications/de-icing-of-multi-layer-composite-plates-using-ultrasonic-guided–2 Accessed 2021-05-08

[13] Overmeyer, A., Palacios, J.L., Smith, E.C., Royer, R.: Rotating Testing of a Low-Power, Non-Thermal Ultrasonic De-icing System for Helicopter Rotor Blades. In: SAE 2011 International Conference on Aircraft and Engine Icing and Ground Deicing (2011). https://doi.org/10.4271/2011-38-0098 . https://www.sae.org/content/2011-38-0098/ Accessed 2021-05-08

[14] Palacios, J.L.: A review of ultrasonic vibration for de-icing of aircraft. In: International Conference on Vibration and Vibro-acoustics, China (2014)

[15] Fink, M.: Time reversal of ultrasonic fields. I. Basic principles. IEEE Transactions on Ultrasonics, Ferroelectrics, and Frequency Control **39**(5), 555–566 (1992) https://doi.org/10.1109/58.156174 . Conference Name: IEEE Transactions on Ultrasonics, Ferroelectrics, and Frequency Control

[16] Fink, M.: Time Reversed Acoustics. Physics Today **50**(3), 34–40 (1997) https://doi.org/10.1063/1.881692 . Publisher: American Institute of Physics. Accessed 2021-05-08

[17] Tanter, M., Thomas, J.-L., Fink, M.: Time reversal and the inverse filter. The Journal of the Acoustical Society of America **108**(1), 223–234 (2000) https://doi.org/10.1121/1.429459 . Accessed 2021-07-08

[18] Anderson, B.E., Douma, J., Ulrich, T.J., Snieder, R.: Improving spatio-temporal

focusing and source reconstruction through deconvolution. Wave Motion **52**, 151–159 (2015) https://doi.org/10.1016/j.wavemoti.2014.10.001 . Accessed 2021-07-08

[19] Derode, A., Tourin, A., Fink, M.: Ultrasonic pulse compression with one-bit time reversal through multiple scattering. Journal of Applied Physics **85**(9), 6343–6352 (1999) https://doi.org/10.1063/1.370136 . Publisher: American Institute of Physics. Accessed 2021-05-17

[20] Montaldo, G., Roux, P., Derode, A., Negreira, C., Fink, M.: Generation of very high pressure pulses with 1-bit time reversal in a solid waveguide. The Journal of the Acoustical Society of America **110**(6), 2849–2857 (2001) https://doi.org/10.1121/1.1413753 . Publisher: Acoustical Society of America. Accessed 2021-05-17

[21] Willardson, M.L., Anderson, B.E., Young, S.M., Denison, M.H., Patchett, B.D.: Time reversal focusing of high amplitude sound in a reverberation chamber. The Journal of the Acoustical Society of America **143**(2), 696–705 (2018) https://doi.org/10.1121/1.5023351 . Accessed 2021-06-21

[22] Heaton, C., Anderson, B.E., Young, S.M.: Time reversal focusing of elastic waves in plates for an educational demonstration. The Journal of the Acoustical Society of America **141**(2), 1084 (2017) https://doi.org/10.1121/1.4976070 . Publisher: Acoustical Society of America ASA. Accessed 2021-09-11

[23] Francoeur, D., Berry, A.: Time reversal of flexural waves in a beam at audible frequency. The Journal of the Acoustical Society of America **124**(2), 1006–1017 (2008) https://doi.org/10.1121/1.2945160 . Accessed 2021-05-08

[24] Gemmeren, V., Zybach, B., Dual, J.: Focusing Flexural Waves in Beams for Precisely Controlled Dynamic Fracture. Physical Review Applied **10**(4) (2018) https://doi.org/10.1103/PhysRevApplied.10.044021 . Accessed 2021-05-04

[25] Waters, T.P.: A chirp excitation for focussing flexural waves. Journal of Sound and Vibration **439**, 113–128 (2019) https://doi.org/10.1016/j.jsv.2018.07.028 . Accessed 2021-05-08

[26] Raffaele, D., Waters, T.P., Rustighi, E.: Wave propagation in an aircraft wing slat for de-icing purposes. In: MEDYNA2020: 3rd Euro-Mediterranean Conference on Structural Dynamics and Vibroacoustics, Napoli, p. 4 (2020). https://medyna2020.sciencesconf.org/

[27] Raffaele, D., Rustighi, E., Waters, T.: Semi-Analytical Finite-Element Analysis for Free and Forced Wave Propagation Using COMSOL and LiveLink for Matlab. Vibration **6**(2), 359–374 (2023) https://doi.org/10.3390/vibration6020022 . Number: 2 Publisher: Multidisciplinary Digital Publishing Institute. Accessed 2023-08-06

[28] Raffaele, D.: Focussing elastic waves in wing leading edge structures. PhD thesis, University of Southampton (2022). https://eprints.soton.ac.uk/470116/ Accessed 2024-09-22

[29] Mace, B.R., Manconi, E.: Wave motion and dispersion phenomena: Veering, locking and strong coupling effects. The Journal of the Acoustical Society of America **131**(2), 1015–1028 (2012) https://doi.org/10.1121/1.3672647 . Accessed 2021-12-16

[30] Bois, J.L., Adhikari, S., Lieven, N.: Experimental and Numerical Investigation of Mode Veering in a Stressed Structure. International Modal Analysis Conference (2007)

[31] Bartoli, I., Marzani, A., Scalea, F., Viola, E.: Modeling wave propagation in damped waveguides of arbitrary cross-section. Journal of Sound and Vibration **295**(3-5), 685–707 (2006) https://doi.org/10.1016/j.jsv.2006.01.021 . Accessed 2021-05-04

[32] Carcione, J.M.: Wave Fields in Real Media: Wave Propagation in Anisotropic, Anelastic, Porous and Electromagnetic Media, 4th edn. Elsevier

[33] Clayton, R.W., Wiggins, R.A.: Source shape estimation and deconvolution of teleseismic bodywaves. Geophysical Journal International **47**(1), 151–177 (1976) https://doi.org/10.1111/j.1365-246X.1976.tb01267.x . Accessed 2022-02-22

[34] Lang, G.F., Snyder, D.: Understanding the physics of electrodynamic shaker performance. S V Sound and Vibration **35**, 24–33 (2001)